JOURNAL OF Bio-X Research

RESEARCH ARTICLE

http://dx.doi.org/10.1097/JBR.0000000000000103

OPEN

Antitumor and off-target effects of cholesterol-conjugated let-7a mimics in an orthotopic hepatocellular carcinoma xenograft nude mouse model

Jian Guan[a,*], Mingyang Liu[b], Xin Li[c,d], Liangrui Zhou[b], Xueyu Dong[e], Wei Dai[f], Yu Xia[g], Tao Yang[a,b], Shaojuan Guo[a], Xingqi Li[b], Yehua Han[f], Yufeng Luo[b]

Abstract

Objective: To explore the antitumor and potential off-target effects of systemically delivered cholesterol-conjugated *let-7a* mimics *(Chol-let-7a)* and control mimics *(Chol-miRCtrl)* on hepatocellular carcinoma *in vivo.*

Methods: The antitumor effects of two intravenous dosing regimens of *Chol-let-7a* on heptocellular carcinoma growth were compared using an orthotopic xenograft mouse model. Off-targets were analyzed with histopathological and ultrapathological features of heparenal tissue and cells in the *Chol-let-7a-, Chol-miRCtrl-,* and saline-treated (blank) xenograft mice and normal control mice. Then, *let-7*a abundance in orthotopic tumors, corresponding paracancerous hepatic tissue, and normal liver tissue from healthy nude mice was examined by reverse transcription-polymerase chain reaction. The distribution of *Chol-let-7a* and *Chol-miRCtrl in vivo* was examined by whole-animal imaging and frozen-sections observation. The experiments were approved by the Institutional Research Board of Peking Union Medical College Hospital.

Results: Continuous treatment with *Chol-let-7a* resulted in tumors that were 35.86% and 40.02% the size of those in the *Chol-miRCtrl* and blank xenograft group ($P < 0.01$ and $P < 0.01$, respectively), while intermittent dosing with *Chol-let-7a* resulted in tumors that were 65.42% and 56.66% the size of those in the *Chol-miRCtrl* and the blank control group, respectively ($P < 0.05$ and $P < 0.05$). In addition, some histopathological and ultrapathological features were only observed after treatment with the two cholesterol-conjugated molecules, however mild with intermittent dosing *Chol-let-7a* treatment, such as diffuse sinusoidal dilation and edema, primarily around the centrolobular vein in heptic tissues; mild hypercellularity with dilated capillary lumens in the renal tissue; and some organelle abnormalities found in heptic and renal cells. Furthermore, whole-animal imaging showed that *Chol-let-7a* and *Chol-miRCtrl* were predominantly distributed in the liver, kidney, and bladder regions after injection, and that the concentration of *Chol-let-7a* and *Chol-miRCtrl* in the kidney and the bladder decreased much slowly in the xenograft animals, especially in the *Chol-miRCtrl* group. Finally, RT-PCR analysis showed that *let-7a* levels were significantly increased in Chol-let-7a-treated xenografts compared with *Chol-miRCtrl* group (P=0.003) and blank xenograft group (P=0.001); however, the level was only equivalent to 50.6% and 40.7% of that in paracancerous hepatic tissue and hepatic tissue in normal mice, respectively.

Conclusions: *Chol-let-7a,* administered either continuously or intermittently, showed effective antitumor efficacy. *Chol-let-7a* had some off-target effects, such as mild acute hepatitis-like inflammation and non-specific drug-induced kidney injury. The intermittent dosing regimen resulted in less damage than the continuous regimen, while maintaining relatively satisfactory antitumor efficacy, which could be useful for the investigation and possible clinical use of miRNA treatment regimens in the future.

Keywords: drug-induced renal injury, hepatic toxicity, *in vivo* off target effects, *let-7* mimics, nonviral delivery vector

Supplemental Digital Content is available for this article.

JG and ML contributed equally to the writing of this article.

[a] The National Population and Health Scientific Data Centre (Clinical Medicine), [b] Department of Pathology, [c] Department of Nuclear Medicine, Peking Union Medical College Hosptial, Chinese Academy of Medical Sciences (CAMS) and Peking Union Medical College (PUMC), Beijing, [d] Department of Nuclear Medicine, The Cancer Hospital of the University of Chinese Academy of Sciences (Zhejiang Cancer Hospital), Institute of Basic Medicine and Cancer (IBMC), Chinese Academy of Sciences, Hangzhou, Zhejiang Province, [e] National Laboratory of Medical Biology, Institute of Basic Medical Sciences, [f] The Electron Microscope Laboratories Center, Institute of Basic Medical Sciences, [g] Department of Ultrasound, Peking Union Medical College Hospital, Chinese Academy of Medical Sciences (CAMS) and Peking Union Medical College (PUMC), Beijing, China

** Corresponding author: Jian Guan, the National Population and Health Scientific Data Centre (Clinical Medicine), Peking Union Medical College Hospital, CAMS/PUMC, No. 1, Shuaifuyuan Street, Dongcheng District, Beijing 100730, China. E-mail: gjpumch@126.com.*

Journal of Bio-X Research (2022) 5:181–196

Received: 5 March 2021; Accepted: 12 July 2021

Published online 24 August 2021

http://dx.doi.org/10.1097/JBR.0000000000000103

Introduction

Hepatocellular carcinoma (HCC) is the fifth most common cancer worldwide and the third most common cause of cancer mortality.[1] It is the second leading cause of cancer-related death to lung cancer in China.[2] There is a high recurrence rate of HCC after surgery, and chemotherapy and radiotherapy have limited efficacy for HCC and are associated with serious toxicity.[1,3] Thus, new therapeutic strategies for HCC are urgently needed, especially for advanced-stage patients.

MicroRNAs (miRNAs) are endogenous, non-coding, small RNAs that repress gene expression at the post-transcriptional level by base pairing to the 3'-untranslated region of target messenger RNAs, and are important mediators of carcinogenesis and predictors of clinical prognosis.[4–6] Functional studies have confirmed that miRNAs act as tumor suppressors and are dysregulated in many types of cancer. Thus, modulating miRNAs represents a promising new tool for cancer therapy.[7,8] The *let-7* family of miRNAs function as typical miRNA tumor suppressors in their ability to target multiple mRNAs, which makes them interesting candidates for development as miRNA mimic-based therapeutics.[9]

In recent years, both viral and nonviral delivery vehicles have been developed for the delivery of RNA, including the miRNA gene or mimics *in vivo*.[10,11] However, both types remain challenges for potential clinic use in the future. As an example of viral delivery, the adeno-associated virus (AAV) vector for miRNA delivery has low efficiency in terms of miRNA expression, and provokes an immune reaction in response to the viral proteins, and shows dose-dependent toxicity in patients, all of which pose significant hurdles to its potential clinical use. In addition, AAV-mediated recombinant miRNA gene expression in target cancer cells decreases rapidly as the non-replicating episomal viral genome is lost from the cells.[12] Nonviral vehicles that have been tested *in vivo* involve the use of miRNA mimic modifications or carriers that facilitate release from endosomes, thereby improving delivery to target cells and potentially increasing the therapeutic effects. Using nonviral delivery vehicles, miRNA mimics, such as those mimicking the *miR-122* and *let-7* miRNA families, have shown effective anti-HCC efficacy *in vivo* in preclinical studies.[13,14]

Among the delivery system, some RNA-based drugs are modified with 3′ cholesterol that can aid the association of the siRNA to lipoprotein particles, lipoprotein receptors and transmembrane proteins, and thus target the siRNA to specific tissues, such as the liver.[10] In addition, as an essential component of animal cell membranes, and, cholesterol is an efficient transmembrane transporter and considered non-toxic. We previously showed that cholesterol-conjugated *let-7a* (*Chollet-7a)* exerted significant antitumor effects by down-regulating all three human *ras* genes *in vivo,* including *n-ras, k-ras, and h-ras*. However, our *in vitro* experiments also suggested that cholesterol-conjugated miRNA mimics have potential off-target effects, as indicated by morphological differences between cells treated with a negative control miRNA mimic *(Chol-miRCtrl)* and untreated tumor cells. Compared to untreated (blank) tumor cells, the *Chol-miRCtrl*-treated cells exhibited decreased survival and viability.[15] The potential off-target effects that may occur *in vivo* remain unknown; and it is crucial for off-target effects to be minimized when using this approach. In this study we investigated the antitumor efficacy and potential off-target effects of cholesterol-conjugated *let-7a* miRNA delivered by either a continuous or an intermittent dosing regimen, to provide important information for the future study and potential clinical use of miRNA mimics.

Materials and methods

Experimental animals and miRNAs

All *in vivo* experiments were performed in accordance with the Guide for the Care and Use of Laboratory Animals (NIH Publication No. 85-23, revised 1996) and the experimental animal welfare ethics regulations of China, with the approval of the Institutional Research Board, Peking Union Medical College Hospital. All animal experiments were performed at the Centre for Experimental Animal Research (SPF cleanliness, license No. SYXK (Jing) 2010-0021, Beijing, China), Institute of Basic Medical Sciences (IBMS), CAMS & PUMC.

BALB/C nude (nu/nu) mice (6-7 weeks old, 20 ± 3g) were purchased from the National Institutes for Food and Drug Control (lot No. 11400500001092; Beijing, China). The cholesterol-conjugated *let-7a (Chol-let-7a)* and negative control miRNA (*Chol-miRCtrl)* mimics were purchased from Ribobio (Guangzhou, China).

Orthotopic xenograft nude mouse model

HepG2 cells (2×10^6) were injected directly into the livers of 20 nude mice. One week later, the formation of HepG2 orthotopic xenografts was confirmed by ultrasonography using a Vevo 2100 high-frequency ultrasound system (VisualSonics, Inc. Beijing, China). Fifteen successfully engrafted mice were randomized into three cohorts of five animals.

Assessment of antitumor and off-target effects of cholesterol-conjugated molecules administered continuously or intermittently

Two dosing regimens were designed to evaluate the antitumor efficacy and off-target effects of *Chol-let-7a* and *Chol-miRCtrl.*

We first evaluated the effects of continuous delivery of *Chol-let-7a* on HepG2 orthotopic xenografts in nude mice.'10' The mice were injected with *Chol-let-7a* or *Chol-miRCtrl* (5nmol in 250 µL saline) via the tail vein every 3 days for 5 weeks, after which the tumor size (volume, mm) and changes in liver and kidney tissues and cells were observed. Xenograft mice injected with the same volume of 0.9% physiological saline were used as the negative xenograft control (blank) group.

To observe the effects of the cholesterol-conjugated molecules on normal mice in the absence of tumor, 10 nude mice were randomized to two groups of five animals each and injected with *Chol-let-7a* or *Chol-miRCtrl* according to the dosing regimen described above.

To assess the effects of intermittent dosing, mice with orthotopic xenografts and normal nude mice were injected with *Chol-let-7a, Chol-miRCtrl,* or saline as above every 3 days for 2 weeks, left uninjected for 1 week, and then injected every 3 days for another 2 weeks.

At the end of the 5-week experimental period for all groups, tumor size was measured on three orthogonal axes *(a, b,* and *c),* and tumor volumes (mm^3) were calculated according to the following formula: $V = (abc)/2$.[16] Samples of tumor, liver, kidney, and other tissues from all animals were harvested and snap-frozen or preserved in 10% neutral buffered formalin rapidly for further examination.

Histopathological examination under light microscope

All samples fixed in 10% neutral buffered formalin were routinely processed and embedded in paraffin; and were submitted for standard processing with hematoxylin and eosin staining (HE), Histopathological features was evaluated with HE sections observed under histopathological examination under the light microscope (LM) (OLYMPUS Corporation, Japan).

Transmission electron microscopy

Fresh and snap-frozen tissues were fixed with 2.5% glutaraldehyde for 30 minutes at room temperature, followed by 1.5 hours in 2% OsO_4. Samples were stained and examined with a transmission electron microscope (JEOL JEM 1010, Tokyo, Japan), and digital images were obtained with an Erlangshen ES1000W camera (Model 785, Gatan, Warrendale, PA, USA).

In vivo whole-animal imaging and distribution analysis

Fluorophore-labeled synthetic *Chol-let-7a* or *Chol-miRCtrl* (RiboBio, Guangzhou, China) was administered via the tail vein. Two mice with HepG2 orthotopic xenografts were injected with Cy5-labeled *Chol-let-7a,* two mice with HepG2 orthotopic xenografts were injected with Cy5-labeled *Chol-miRCtrl,* two normal nude mice were injected with Cy5-labeled *Chol-let-7a,* and two normal nude mice were injected with Cy5-labeled *Chol-miRCtrl.* Whole-animal images were recorded at 15, 45, 60, and 100 minutes, and 19, 24, 48, and 72hours after treatment using the NightOWL LB 983 *in vivo* imaging system (Berthold, Beijing, China). Digital images were produced and analyzed with Indigo software (Berthold).

In vitro con foca and phase fluorescence microscopy

Two pairs of xenograft mice and two pairs of normal mice were injected with Cy5-labeled *Chol-let-7a* or *Chol-miRCtrl* (5nmol in 250 μL saline buffer). Fresh orthotopic tumor and liver tissues were snap-frozen 2 hours after injection of *Chol-let-7a* or *Chol-miRCtrl.* Frozen sections with a thickness of 10-20 μm were observed and imaged using a confocal laser scanning microscope (OLYMPUS FV1000, OLYMPUS Inc., Shanghai, China) and a phase fluorescence microscope (Leitz, Laborlux 12).

Quantification of let-7a miRNA expression

Total miRNA was isolated from snap-frozen HepG2 xenograft tumor and paracancerous liver tissue using a mirVANA™ PARIS™ RNA isolation kit (Applied Biosystems, Carlsbad, CA, USA). RNA (10 ng) was reverse-transcribed using a miRNA Reverse Transcription Kit (Applied Biosystems) and *let-7a*-specific primers (TaqMan miRNA Assay, Applied Biosystems).

Quantitative real-time PCR was performed with an ABI Prism 7500 Sequence Detection System (Perkin-Elmer Applied Biosystems, Foster City, USA) and the Perkin-Elmer Biosystems analysis software according to the manufacturer's instructions. RNU6B was used as a housekeeping control gene. Relative expression was calculated using the $2^{-\Delta\Delta CT}$ method.[17]

Determination of serum cytokines

Twelve normal nude mice and twelve mice with HCC orthotopic tumors were injected with either *Chol-let-7a* or *Chol-miRCtrl* (n = 6 per group) every 3 days for 4 weeks, beginning 1 week after the HepG2 cells were implanted. Serum samples were obtained from the tail vein at the beginning and end of the 4-week experimental period, and the levels of four cytokines interleukin-6 (IL-6), interleukin-8 (IL-8), tumor necrosis factor-alpha (TNF-α), and vascular endothelial growth factor (VEGF) were quantified by multiplex assays. Cytokine levels (IL-6, IL-8, TNF-α, and VEGF) in blood serum samples (200 μL) were quantified with ELISA using a commercial kit (96-Well Plate MILLIPLEX® MAP, Merck Millipore, Darmstadt, Germany) and a Lunimex 200 instrument (MILLIPLEX®, Germany). The data were analyzed using Milliplex Analyst software.

Serum samples were obtained prior to and after *Chol-let-7a* or *Chol-miRCtrl* administration, and the levels of four cytokines were examined. The cytokine levels are shown in Additional Table 1 (http://links.lww.com/JR9/A31).

Statistical analysis

Data are expressed as the mean ± SEM. All data analyses were performed using SPSS 16.0 software (SPSS, Chicago, IL, USA). Student's t-test was used for statistical comparisons between groups. $P < 0.05$ was considered to be statistically significant.

Results

Antitumor efficacy of Chol-let-7a in orthotopic xenograft models

Orthotopic tumor sizes were evaluated at the end of 5 weeks of treatment with the continuous or intermittent dosage regimen (Fig. 1). The tumor size (volume, mm^3) in the continuous-dosage *Chol-let-7a-treated* xenograft group was 152.15 ± 38.43, which was 35.86% ($P < 0.01$) and 40.02% ($P < 0.01$) the size of the tumors in the two control groups *(Chol-miRCtrl,* 424.34 ± 60.10; blank xenograft group, 380.23 ± 74.83). At the end of the intermittent treatment regimen, the tumor sizes in the *Chol-let-7a*-treated, *Chol-miRCtrl*-treated, and blank xenograft group were 163.66 ± 25.81, 250.16 ± 44.91, and 288.85 ± 38.59, respectively; the tumors in the *Chol-let-7a* treated mice were significantly smaller than those in the *Chol-miRCtrl-treated* and blank xenograft groups, at 65.42% ($P = 0.012$) and 56.66% ($P = 0.031$), respectively. There was no significant difference in tumor size in the *Chol-miRCtrl* and blank xenograft groups ($P = 0.23$).

Effects of Continuous administration of Chol-let-7a or Chol-miRCtrl on the liver and kidney in xenograft and normal mice

LM and transmission electron microscopy analysis of hepatic tissues and cells

Hepatic tissues from xenograft mice and control mice were observed after continuous administration of *Chol-let-7a, Chol-miRCtrl* and saline only (blank) for 5 weeks. LM analysis (Fig. 2) showed diffuse, chronic, nonspecific inflammation in the liver parenchyma of all three xenograft mice. Spotty and focal necrosis and mass lesions/confluent necrosis were observed. The necrosis was milder in the *Chol-let-7a*-treated group than in the two xenograft control groups. Significant diffuse sinusoidal dilation and edema, primarily around the centrolobular vein, were observed in the *Chol-let-7a*-and *Chol-miRCtrl-treated* groups. Higher magnification showed sinusoidal endothelial cell hyperplasia in the *Chol-let-7a-,* and *Chol-miRCtrl-treated* xenograft mice; and

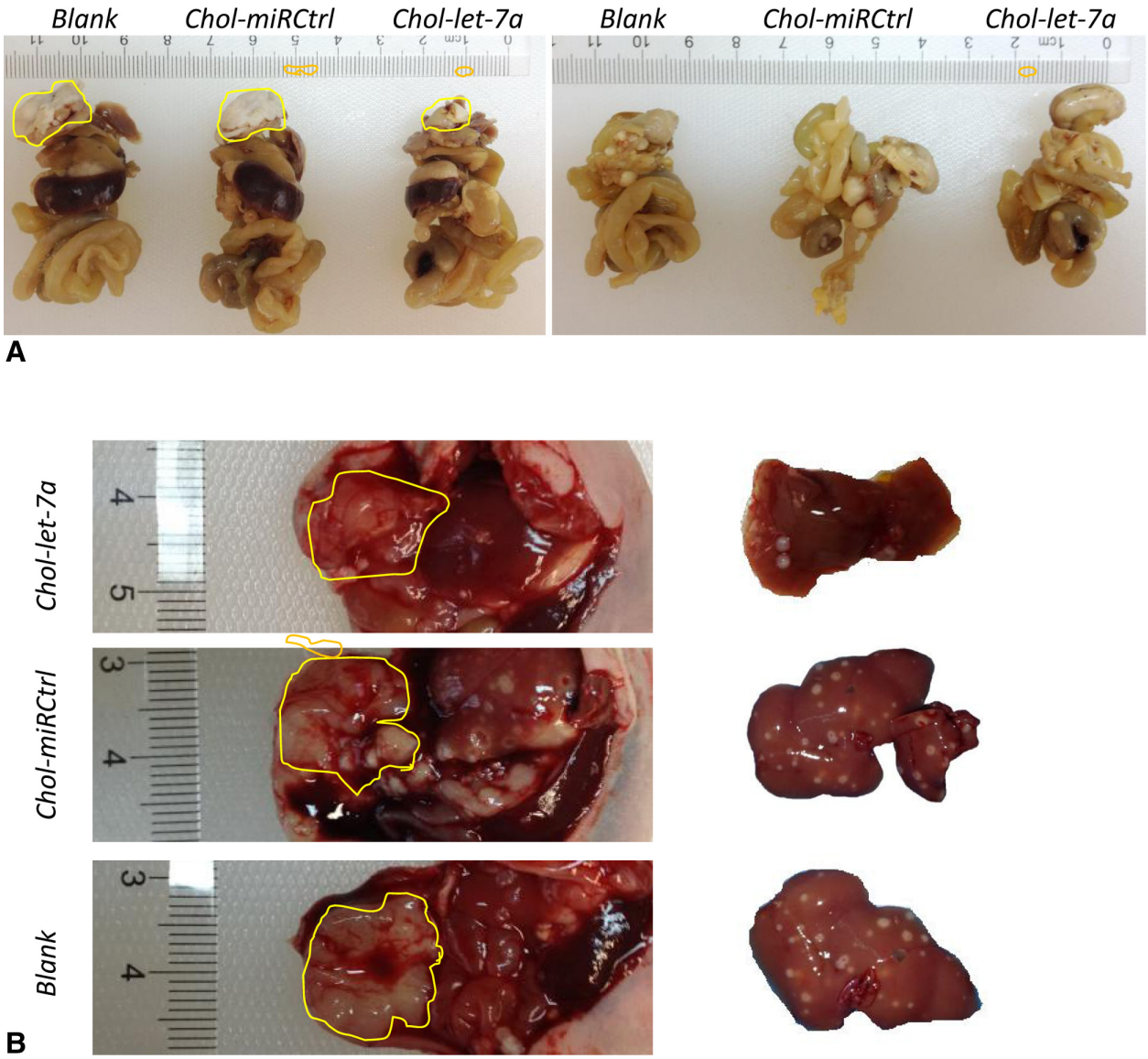

Figure 1. Orthotopic tumor growth and metastasis inhibited by systemic treatment with *Chol-let-7a.* To assess antitumor efficacy *in vivo,* we evaluated the effects of *Chol-let-7a,* administered via a continuous or intermittent dosage regimen, on HepG2 orthotopic xenografts in nude mice. Orthotopic tumor size was evaluated at the end of 5 weeks. Gross specimen analysis showed that both dosing regimens inhibited tumor growth (area in the yellow band) and metastasis. (A) Continuous dosing regimen. (B) Intermittent dosing regimen.

significant centrolobular vein congestion and necrosis was predominantly observed in the *Chol-miRCtrl* and blank xenograft groups (Fig. 3A). In addition, focal irregular sinusoidal dilation with congestion was found primarily in the *Chol-miRCtrl* and blank xenograft groups, along with some leukocyte infiltration.

Sinusoidal and perisinusoidal lumen dilation in the hepatic tissue from *Chol-let-7a-* and *Chol-miRCtrl*-treated was confirmed by transmission electron microscopy (TEM) (Fig. 3B). The tissue samples from some of these mice exhibited disrupted hepatic sinusoid structure (3/5 *Chol-let-7a-treated* mice; 4/5 *Chol-miRCtrl-treated* mice) and hepatic sinusoid fibrosis (2/5 *Chol-let-7a*-treated mice; 3/5 *Chol-miRCtrl*-treated mice). In addition, some organelle abnormalities, such as enlarged, irregular, or swollen mitochondria, autophagic bodies, and multilamellar bodies, were observed in the hepatocyte cytoplasm (4/5 *Chol-let-7a*-treated mice; 4/5 *Chol-miRCtrl*-treated mice) (Fig. 3C).

The same experiment was performed in normal nude mice to exclude the effects of xenograft tumor growth. In hepatic tissue from these mice, diffuse sinusoidal dilation was observed after *Chol-let-7a-* and *Chol-miRCtrl* treatment. However, the inflammation and necrosis were significantly milder than in the xenograft mice (Fig. 2). LM analysis of the hepatic tissue showed chronic inflammation and fibrosis, along with nonspecific focal degeneration and necrosis or focal or spotty apoptotic hepato-cytes (Fig. 2). Discontinuous central lobular veins and bile ducts accompanied by non-specific reactive cell proliferation and inflammatory cell infiltration were occasionally observed.

LM and TEM analysis of renal tissues and cells

Renal tissues and cells from xenograft and normal mice treated continuously with *Chol-let-7a* or *Chol-miRCtrl* were then assessed by LM and TEM.

LM analysis of renal tissue showed mild inflammatory cell infiltration and interstitial alterations, such as intertubular blood capillary dilation and intertubular hemorrhage, in all three xenograft

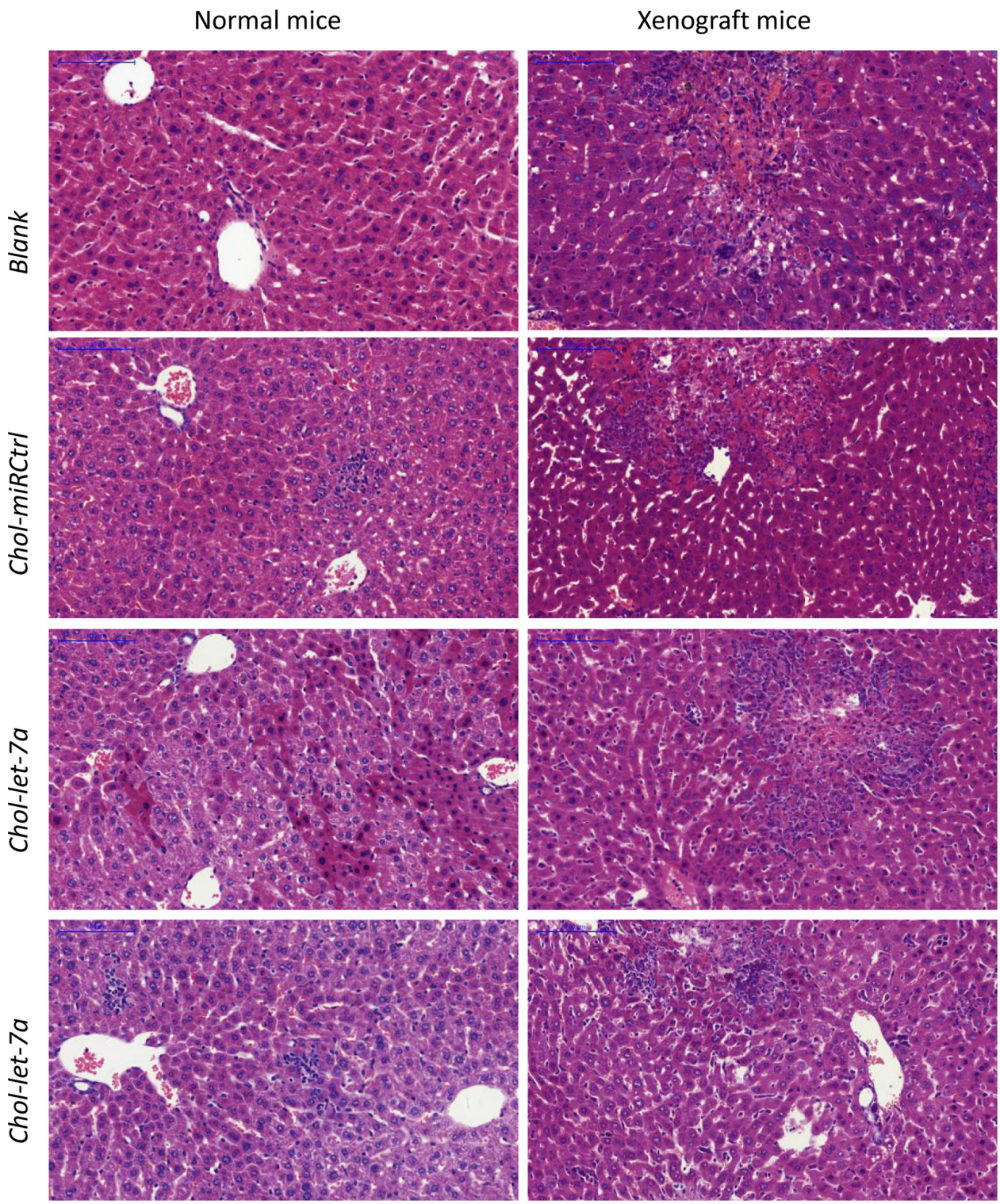

Figure 2. Light microscope images of liver sections from xenograft and normal mice after continuous treatment with *Chol-let-7a* or *Chol-miRCtrl.* The images show focal necrosis and mass lesions in the xenograft mice, and diffuse sinusoidal dilation in the *Chol-let-7a-* and *Chol-miRCtrl-treated* xenograft mice and normal mice under hematoxylin-eosin staining. Scale bars = 100 mm.

groups. These effects were relatively mild in the *Chol-let-7a*-treated group. Dilated glomerular lumens, renal cell dissociation, and renal tubule necrosis were seen in all three xenograft groups under high magnification. Focal segmental sclerotic glomeruli were occasionally observed in the blank xenograft mice. Congested glomeruli and intertubular blood capillary dilation were predominantly observed in the *Chol-miRCtrl-treated* and blank xenograft control mice. No significant congestion was observed in the *Chol-let-7a*-treated group. However, mild hypercellularity with dilated patent capillary lumens was observed in the *Chol-let-7a-* and *Chol-miRCtrl*-treated mice. Congestion and hypercellularity were observed in the *Chol-miRCtrl*-treated and blank xenograft mice.

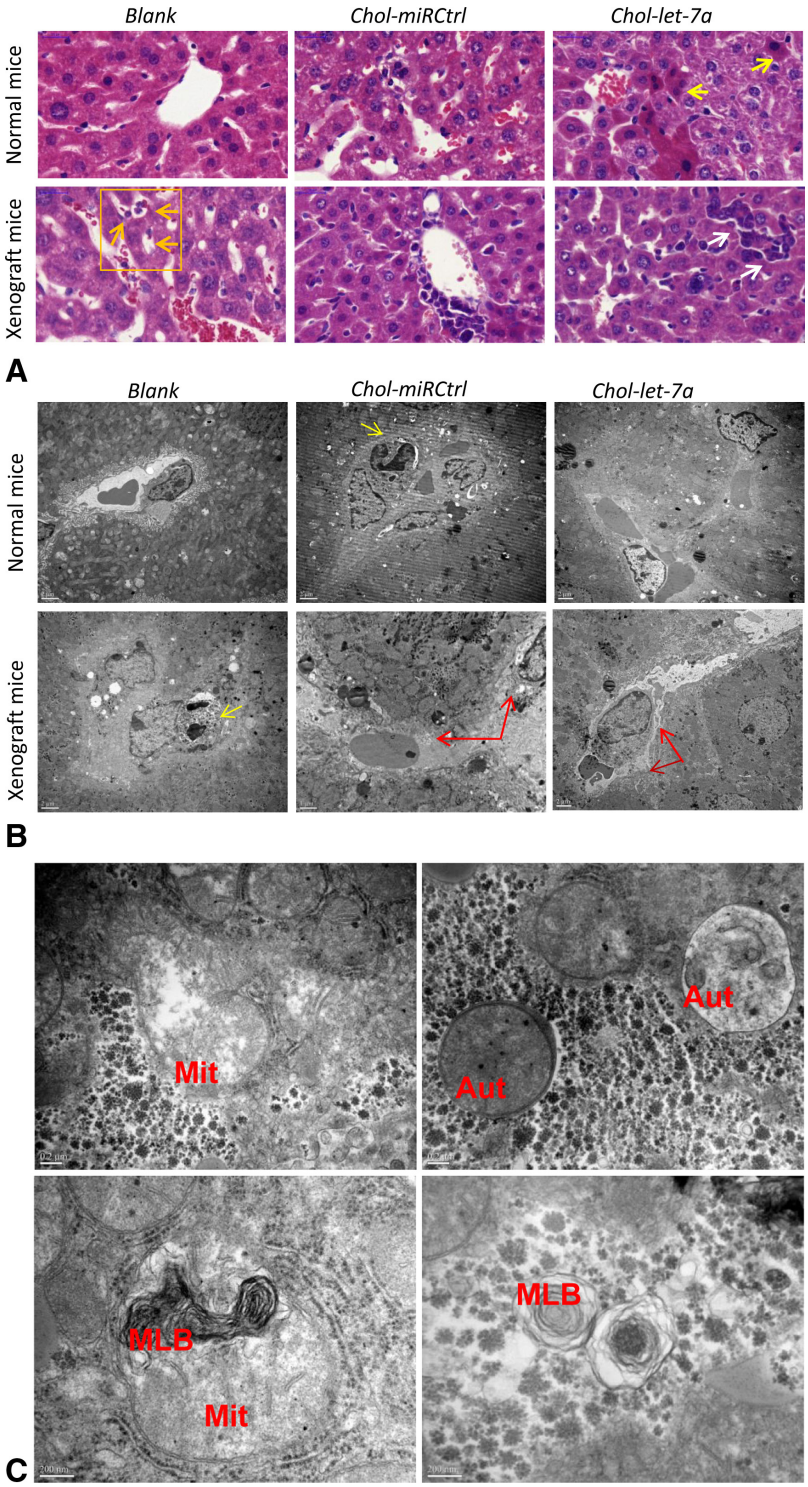

Figure 3. Liver histopathology and ultrastructural features after continuous therapy. (A) Light microscopy findings under high magnification. The images show dilated sinusoids. Also shown are sinusoidal endothelial cell hyperplasia (white arrows); mild focal and spotty apoptotic cells (yellow arrows); and inflammatory cells (orange arrows) under hematoxylin-eosin staining. Scale bars = 20 μm. (B) Transmission electron microscopy (TEM) images of hepatic sinusoidal structures. The images show edematous and dilated sinusoidal and perisinusoidal lumens with structural damage and mild fibrosis of the hepatic sinusoids (red arrows) in the *Chol-let-7a*- and *Chol-miRCtrl-treated* groups. Also shown are leukocytes (yellow arrows) in the *Chol-miRCtrl-treated* and blank control groups. Scale bars = 2 μm. (C) Ultrastructure of liver parenchymal cells after continuous treatment with *Chol-let-7a* (TEM). Here shows some organelle abnormalities, enlarged, irregular, swollen mitochondria (Mit); autophagic bodies (Aut), and multilamellar bodies (MLB) observed in the hepatocyte cytoplasm. Scale bars = 200 nm.

The features described above were confirmed by TEM (Fig. 4). Congestion was primarily observed in the glomerular capillaries and proximal tubule interstitia in the *Chol-miRCtrl*-treated and blank xenograft mice; inflammatory cells were also more prevalent in the glomeruli in the two control groups. As shown in Figure 4A and B, some features were similar in the xenograft

mice after *Chol-let-7a* and *Chol-miRCtrl* treatment. The features and their incidence rate in *Chol-let-7a*- and *Chol-miRCtrl*-treated mice were: glomerular features such as dilated lumens and endocapillary membrane hyperplasia (5/5, 5/5) and focal foot[5] process effacement and focal basement membrane thickening (3/5, 2/5). In addition, inclusion bodies (4/5, 5/5) were readily apparent in the glomerular capillary endothelial cells (Fig. 4A and B). The tubule cells exhibited abnormal mitochondria (Mit) (4/5, 4/5), multilamellar bodies (MLBs)[7] (3/5, 3/5), and autophagic bodies (Aut) (3/5, 4/5) (Fig. 4A and C). However, dilated and destroyed interstitial structures with inflammatory cell infiltration, as well as mild tubulitis, were observed in all three xenograft groups (Fig. 4A).

In normal mice, the congestion and inflammation were mild. However, hyperplasia of the glomerular endocapillary cell membrane (3/4, 3/4) and the presence of inclusion bodies in glomerular capillary endothelial cells were observed in *Chol-let-7a*- and *Chol-miRCtrl-treated* mice (3/4, 3/4) (Fig. 4A). Inflammatory cells were occasionally observed in the dilated glomerular lumen in *Chol-let-7a* and *Chol-miRCtrl*-treated normal mice (2/4, 1/4) (Fig. 4A).

The LM and TEM findings regarding off-target effects of this cholesterol-conjugated delivery system are summarized in Tables 1 and 2.

Effects of intermittent administration of Chol-let-7a or Chol-miRCtrl on the liver and kidney in xenograft and normal mice

Next, we examined the effects of injection with *Chol-let-7a, Chol-miRCtrl,* or a saline treatment as blank control on the livers and kidneys of xenograft and normal mice, and compared the findings to those from mice that received the continuous dosing regimen.

Inflammation and mass necrosis were observed in the two control xenograft mouse groups *(Chol-miRCtrl*-treated and blank xenograft); mild inflammation and focal and spotty necrosis were observed in the *Chol-let-7a*-treated mice. Under TEM, organelle abnormalities were occasionally observed in the hepatic parenchymal cells in all xenograft mice. However, only mild, non-specificinflammation was observed in normal mice after injection of *Chol-let-7a* or *Chol-miRCtrl.*

Diffuse sinusoidal dilation and edema and mild sinusoidal endothelial cell hyperplasia were observed in the *Chol-let-7a*- and *Chol-miRCtrl*-treated xenograft and normal mice (Fig. 5A), but at milder levels than those observed in the mice that received the continuous dosing regimen.

Analysis of the renal tissues and cells revealed a similar trend. Mild glomerular inflammation and interstitial lesions were observed in the renal tissues of all of the xenograft mice under LM, and the changes were mild in the *Chol-let-7a*-treated group. However, significant congestion was observed in the glomeruli and tubular interstitia in the *Chol-miRCtrl*-treated group and the blank xenograft group (Fig. 5B). TEM analysis showed significant deposition of blood cells in the dilated glomerular capillaries in the *Chol-miRCtrl*-treated mice and blank xenograft mice (Fig. 5B). Mild membrane hyperplasia of the glomerular capillary walls and the presence of inclusion bodies in the glomerular capillary endothelial cells were observed in the *Chol-let-7a*- and *Chol-miRCtrl*-treated xenograft mice (4/4, 3/4). Mild dilation of the capillary lumens was seen in the *Chol-let-7a*- and *Chol-miRCtrl*-treated normal mice (3/4, 2/4) (Fig. 5B). Occasional irregular organelles were observed in the proximal tubular cells (data not shown).

Let-7a distribution and abundance in xenograft tumors and hepatic tissues after Chol-let-7a treatment

Whole-animal imaging and frozen section analysis

Whole-animal imaging of nude mice and xenograft mice was performed to observe the distribution of *Chol-let-7a* and *Chol-miRCtrl in vivo,* and the overall fluorescence levels of Cy5-labeled *Chol-let-7a* and *Chol-miRCtrl* in the liver and kidney at different time points were analyzed using Indigo software. The whole-animal images showed high concentrations of fluorescence predominantly distributed in the liver, kidney, and bladder from 15 to 100 minutes post-injection (Fig. 6A and B), after which they began to decrease. At 19 hours after administration, the fluorescence was nearly undetectable in the liver, and fluorescence levels in the kidney and bladder region began to decrease.

Beginning at 19 hours after administration, differences in fluorescence levels and distribution among the groups became apparent. The patterns of fluorescence levels in the liver, kidney, and bladder showed similar trends in normal and xenograft mice injected with *Chol-let-7a* and *Chol-miRCtrl.* However, the concentrations of the fluorescently labeled *Chol-let-7a* and *Chol-miRCtrl* in the kidney and bladder decreased much more slowly in the xenograft mice. Moreover, the fluorescence patterns in the livers and kidneys of the xenograft mice differed over time between the *Chol-let-7a* and *Chol-miRCtrl* groups. The fluorescence signal was chiefly concentrated in the hepatorenal region from 15 to 100 minutes. However, the *Chol-let-7a* fluorescence concentration was much stronger than the *Chol-miRCtrl* signal, especially in the liver (Fig. 6C and D). As measured in fluorescence arbitrary units, *Chol-let-7a* fluorescence in the xenograft liver was 4.76 times that seen in *Chol-miRCtrl* xenograft mice, and 9.90 and 7.55 times that seen in *Chol-let-7a*-and *Chol-miRCtrl*-treated normal mice, respectively, at 100 minutes. At 19hours after administration, the fluorescence decreased rapidly, and was nearly undetectable at 48 hours in normal mice, but was still present at relatively high levels in the kidneys and bladders of both xenograft groups. The *Chol-let-7a* and *Chol-miRCtrl* fluorescence levels in the xenograft kidneys were 5.0938 and 4.0938 fluorescence arbitrary units, respectively, which corresponds to 4.77 and 4.08 times of those of the normal controls, respectively (Fig. 6D).

To further compare the fluorescence distribution in orthotopic tumors and adjacent hepatic tissue, frozen sections collected 2 hours post-injection of *Chol-let-7a* or *Chol-miRCtrl* were observed under confocal and phase fluorescence microscopy. In the xenograft mice, fluorescence was observed in both the orthotopic tumor tissues and hepatic tissues, and the intensity was stronger in the tumor tissue than in the corresponding normal hepatic tissue (Fig. 6E).

Next, fluorescence signals were observed in orthotopic tumor and other organ tissue samples taken 2 hours after injection of *Chol-let-7a* or *Chol-miRCtrl* into normal and xenograft mice, using confocal and phase fluorescence microscopy. Strong fluorescence signals were primarily observed in the xenograft tumors, livers, and kidneys from normal and xenograft mice; there was almost no fluorescence seen in other organs, such as the heart, lung, spleen, and pancreas (Fig. 6F). This was consistent with the results from the whole-animal imaging.

RT-PCR results

Using miRNA-specific primers and RT-PCR, we examined *let-7*a abundance in orthotopic tumor tissue, paracancerous hepatic tissue from xenograft mice after 5 weeks of *Chol-let-7a,*

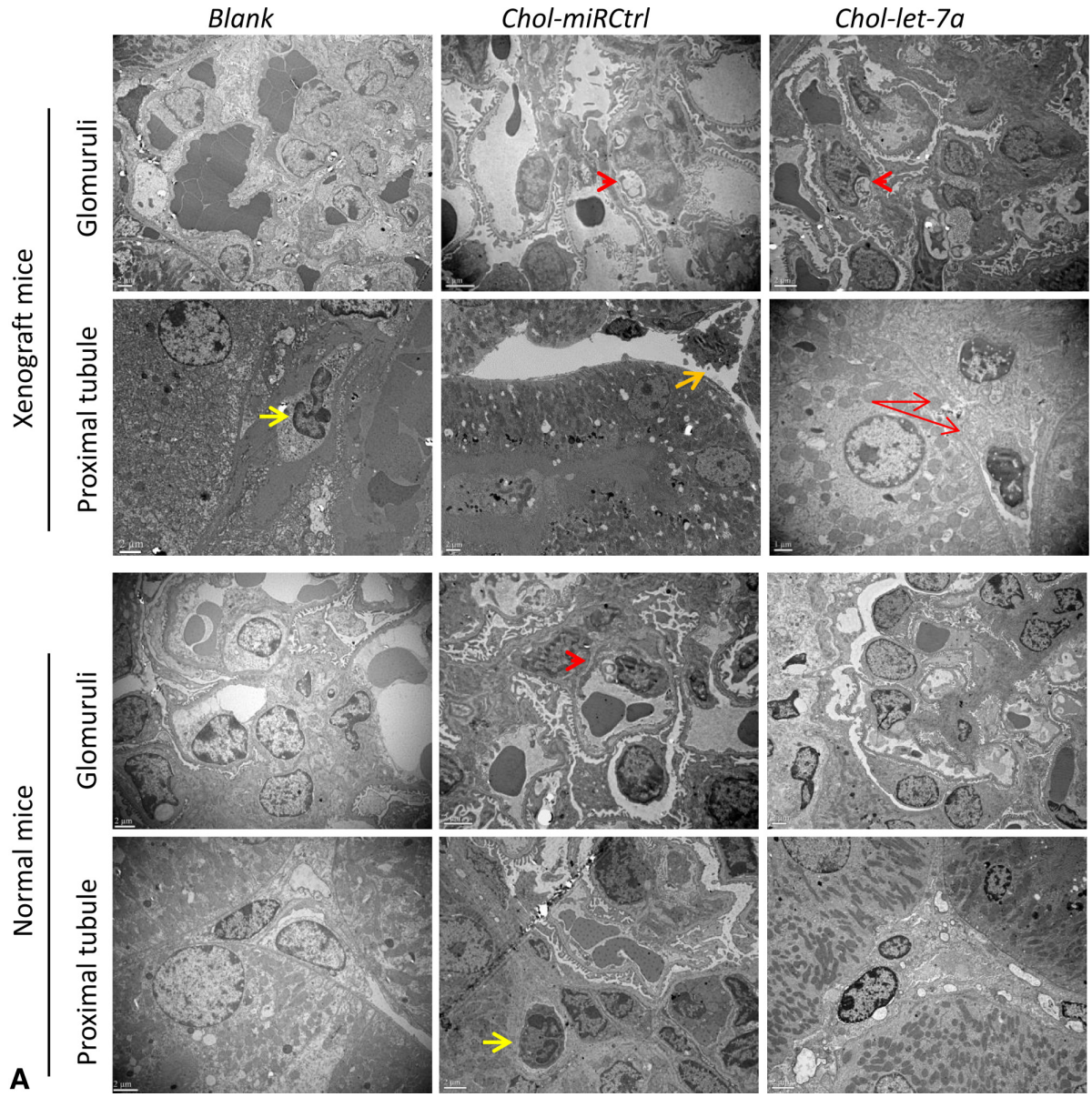

Figure 4. TEM Images of the kidney ultrastructure after continuous treatment. Renal tissues and cells from xenograft and normal mice treated continuously with *Chol-let-7a* or *Chol-miRCtrl* were assessed by TEM. Compared to those in normal mice, congestion was primarily observed in the glomerular capillaries and proximal tubule interstitia in the *Chol-miRCtrl-treated* and blank xenograft mice; inflammatory cells were also more prevalent in the glomeruli in the two control groups. Some features were similar in the xenograft mice after *Chol-let-7a* and *Chol-miRCtrl* treatment. (A) Glomeruli and proximal tubules. The images show inclusion bodies in the glomerular endothelial cells (short red arrows), leukocytes (yellow arrows), and macrophages (orange arrow) in the interstitia, and incomplete interstitial structure (areas between two long thin red arrows). Scale bars = 2 μm. (B) Glomerular changes. Membrane hyperplasia in glomerular capillary cells with bridge structure (wide black arrow) and grid structure (thin black arrow); inclusion bodies (red arrow) in the endothelial cells (En); and focal podocyte (Po) foot process effacement (yellow arrows). Scale bars = 0.5 μm. (C) Changes in proximal tubule cells. Enlarged and irregular mitochondria with vacuoles (white arrows), irregular lysosomes (orange arrow), autophagy (blue arrow), and multilamellar bodies (yellow arrow). Scale bars = 1 μm. TEM = Transmission electron microscopy.

Chol-miRCtrl- and saline (blank) treatment, and heptic tissue from normal mice (Fig. 6G). The *let-7a* levels were significantly higher in *Chol-let-7a-treated* xenografts *(Chol-let-7a* vs *Chol-miRCtrl*, $P = 0.003$; *Chol-let-7a* vs blank xenograft, $P = 0.001$); they were 4.35 and 5.26 times those of the *Chol-miRCtrl*-treated and blank xenograft controls, respectively. There was no significant difference between the two xenograft control groups *(Chol-miRCtrl* vs Blank xenograft, $P = 0.184$). However, the *let-7a* levels in the orthotopic xenografts were still much lower than those seen in the paracancerous hepatic tissue (50.6%) and hepatic tissue in normal mice (40.7%). Moreover, *let-7a* was not significantly up-regulated in the paracancerous hepatic tissue compared to hepatic tissues from normal mice ($P = 0.691$).

Serum cytokines

In the xenograft mice, IL-6 ($P< 0.05$), TNF-α ($P< 0.05$), and VEGF ($P < 0.05$) levels were significantly lower in the *Chol-let-7a*-treated group than in the *Chol-miRCtrl* and blank xenograft groups (Additional Fig. 1A, http://links.lww.com/JR9/A31). Serum IL-8 levels were also decreased in the *Chol-let-7a*-treated group, but the differences were not significant ($P > 0.05$).

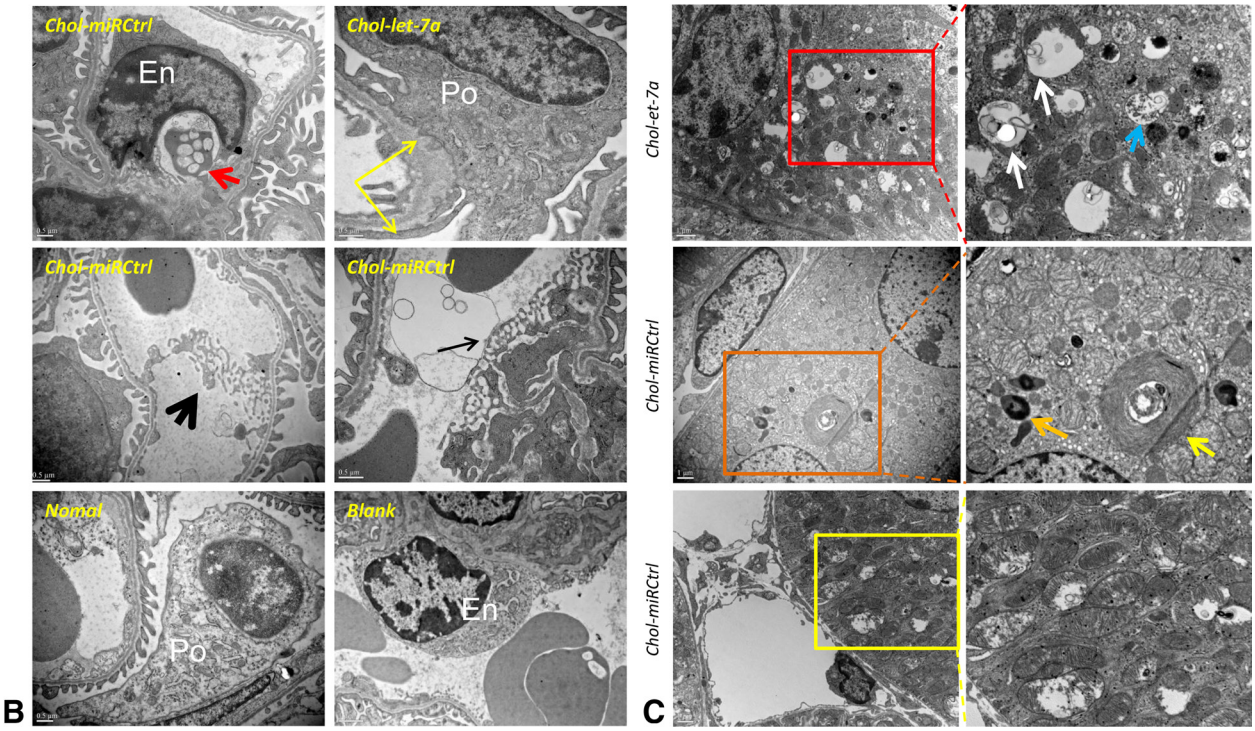

Figure 4. Continued

The levels of IL-6, IL-8, TNF-α, and VEGF in the *Chol-let-7a*- and *Chol-miRCtrl-treated* normal mice were not significantly different from those seen in the normal control mice ($P > 0.05$) (Additional Fig. 1B, http://links.lww.com/JR9/A31). Moreover, we found that IL-6, IL-8, TNF-α, and VEGF levels were significantly increased in the xenograft-only mice in comparison with the normal control mice (Additional Fig. 1C, http://links.lww.com/JR9/A31) (IL-6, $P = 3.885 \times 10^{-5}$; IL-8, $P = 0.0076$; TNF-a, $P = 3.72 \times 10^{-4}$; VEGF, $P = 0.0467$).

Discussion

Antitumor efficacy of Chol-let-7a delivered continuously or intermittently

Previous studies have primarily focused on identifying an effective delivery system for miRNA-based anticancer therapies, which are considered a major obstacle to their clinical use.[11] In clinical practice, a variety of anti-tumor drugs are usually used in combined regimens to decrease the dosage of each medicine used, thereby reducing their untoward effects and avoiding drug resistance. In addition, some drugs are administered intermittently to facilitate tissue and cell repair between doses. Based on this idea, we designed an intermittent dosing regimen for miRNA administration. Our results suggest that both continuous and intermittent *Chol-let-7a* dosing regimens inhibit tumor growth, although the continuous dosing regimen exhibited a greater capacity to shrink the tumors and resulted in fewer intrahepatic and distal (spleen and colon) metastases.

Potential characteristic morphological features of Chol-let-7a off-target effects on the liver and kidney

Safety is an important aspect of drug delivery systems intended for clinic use. The liver and the kidney often show signs of toxicity and injury as a result of exposure to drugs, xenobiotics, or chemicals.[18] Thus, understanding

Table 1

Liver histopathology and ultrastructural changes in normal and xenograft mice after treatment

	Histopathological findings				TEM features				
					Sinusoidal structure				
Group	Inflammation features	Necrosis	Sinusoidal dilation	Congestion	Inflammation features	Irregular organelles	Dilation	Disrupted structures	Cell hyperplasia†
Chol-let-7a-treated normal mice	Mild	Focal /spotty	Diffuse	Mild	Mild (leukocyte)	Yes	Yes	Yes, mild/less	Yes
Chol-miRCtrl-treated normal mice	Mild	Focal /spotty	Diffuse	Mild/Severe	Mild (leukocyte)	Yes	Yes	Yes, mild/less	Yes
Xenograft with no treatment	Severe	Severe	Irregular Focal	Severe	Severe (leukocyte)	No	Mild	Yes	Yes
Cho/-lef-7a-treated xenograft	Mild/severe	Mild/severe	Diffuse	Mild/Severe	Mild Leukocyte	Yes	Yes	Yes	Yes
Chol-miRCtrl-treated xenograft	Severe	Severe	Diffuse	Severe	Severe (leukocyte and macrophage)	Yes	Severe	Yes	Yes

*Organelle abnormalities in parenchymal cells. Sinusoidal endothelial cell hyperplasia. TEM = transmission electron microscopy.

Table 2

Kidney histopathology and ultrastructural changes in normal and xenograft mice after treatment

	Histopathological findings			TEM features						
				Glomeruli				Tubule and tubular interstitia		
Group	Inflammation	Congestion	Dilated lumen of glomeruli	Dilated lumen†	Membrane hyperplasia†	Inclusion bodies†	Congestion	Tubulitis	Congestion Dilation	Dilated Incomplete
Cho/7ef-7a-treated normal mice	Mild	Irregular, mild	Yes	Yes	Yes, mild	Yes	Mild	Mild	Mild	Mild
Chol-miRCtrl-treated normal mice	Mild	Irregular, mild	Yes	Yes	Yes, mild	Yes	Mild	Mild	Mild	Mild
Xenograft with no treatment	Severe	Severe	Severe/focal	Focal	No	No	Severe	Severe	Severe	Focal severe
Cho/7ef-7a-treated xenograft	Mild/severe	Mild	Yes	Mild	Yes, mild	Yes	Mild	Mild	Mild	Mild
Chol-miRCtrl-treated xenograft	Severe	Severe	Yes	Yes	Yes, mild	Yes	Yes, severe	Yes, severe	Yes, severe	Yes, severe

*Membrane hyperplasia of the glomerular capillary wall. †Inclusion bodies in endothelial cells. ‡Dilated and incomplete tubular interstitia. TEM=transmission electron microscopy.

the features and potential mechanism of hepatotoxicity and nephrotoxicity of novel therapeutics is critical for pharmaceutical drug development. Consistent with this, whole-animal imaging showed that *Chol-let-7a* and *Chol-miRCtrl* primarily accumulated in the liver and kidney. Thus, we analyzed these organs in detail to evaluate the potential off-target effects of *Chol-let-7a*.

Histopathology is recognized as the single most appropriate screen for evidence of liver and kidney injury.[14] Cell injury can be noted by electron microscopy examination. Thus, the features of liver and kidney tissues and cells after treatment with the cholesterol-conjugated molecules were observed under LM and TEM to identify the effects of xenograft tumor growth, the delivery system, and up-regulated *let-7a* expression. Features that were only observed in *Chol-let-7a*- and *Chol-miRCtrl*-treated mice, and not found in blank xenograft mice, were considered to represent damage induced by *Chol-let-7a* therapy. Contrary, some histopathological and ultrapathological features that consistent with the growth of xenograft, especially found in blank xenograft mice, were not off-targets of the cholesterol-conjugated molecules,

We summarized and compared the features among the xenograft groups, as well as the differences between the xenograft and normal groups. These results in this study showed that the diffuse simusoidal dilation and edema, and the sinudoidal endothelial cell hyperplasis were related to *Chol-let-7a* and *Chol-miRCtrl* treatment. This was confirmed in the *Chol-let-7a*- and *Chol-miRCtrl*-treated normal mice. The characteristic changes in normal hepatic tissues and cells after administration of the cholesterol-conjugated molecules; however not found in blank xenograft mice, were diffuse sinusoidal dilatation with or without structural damage and sinusoidal lining cell hyperplasia. Similarly, dilation of the glomerular lumen and endocapillary membrane hyperplasia or edematous glomerular capillary and tubular interstitium, often accompanied by inclusion bodies in the glomerular endothelial cells, were primarily induced by injection of the cholesterol-conjugated molecules, *Chol-let-7a* and *Chol-miRCtrl*.

However, all of these features, which were found after *Chol-let-7a* treatment, are non-specific changes that are also produced by other drugs and treatments,[18] including the relative characteristic feature, diffuse sinusoidal dilatation in hepatic tissues, has also been reported in an oral contraceptive-induced liver injury.[19] Similarly, characteristic changes in the renal tissues and cells have also been reported as drug side effect. In addition, the liver and kidney effects were less severe in the intermittent dosing regimen group compared with the continuous regimen.

All these features found in xenograft mice treated with *Chol-let-7a* or *Chol-miRCtrl* exhibited tissue and cell features that are consistent with some common necroinflammatory patterns of drug-induced liver injuries, such as acute (lobular) hepatitis, chronic (portal) hepatitis, and zonal coagulative necrosis, were not characteristic features resulting from *Chol-let-7a* or *Chol-miRCtrl*. Some of the changes were accompanied by spotty and focal parenchyma cell degeneration, apoptosis, or necrosis. Furthermore, these features were aggravated in the corresponding *Chol-miRCtrl-treated* xenograft groups. Congestion and severe acute hepatitis with mass necrosis were mainly accompanied by xenograft tumor growth. In addition, congestion and inflammation were less severe in the *Chol-let7a-treated* xenograft group. To confirm this hypothesis, we examined serum cytokines from xenograft and healthy nude mice to analyze the potential effects of xenograft growth and *Chol-let-7a* on the immune state of nude mice, and to clarify the off-targets from some of the immuno-related changes of *Chol-let-7a* in xenograft mice. Serum cytokine changes in xenograft mice and normal mice after *Chol-let-7a* and *Chol-miRCtrl* suggested that the immune status of the xenograft nude mice affected mostly from the tumor growth. The levels of four cytokines IL-6, IL-8, TNF-α, and VEGF in the *Chol-let-7a*- and *Chol-miRCtrl*-treated normal mice were not significantly different from those seen in the normal control mice ($P > 0.05$). However, the serum levels of IL-6, IL-8, TNF-a, and VEGF in the blank xenograft group were significantly increased in the blank xenograft mice in comparison with the normal control mice.

Analysis of potential off-target effects of Chol-let-7a to liver

MiRNAs target multiple molecules, which could cause side effects at the molecular level *in vivo*. In this study, we analyzed the risks of up-regulating *let-7a* expression in mouse livers. First, we confirmed that *let-7a* was effectively delivered to the xenografted tumor and liver tissues, through *in vivo* whole-animal imaging and *in vitro* frozen section analysis. Under confocal and phase fluorescence microscopy, *Chol-let-7a* fluorescence was observed in both the orthotopic tumor tissues and adjacent liver tissues. The *Chol-let-7a* fluorescence signal was stronger than the *Chol-miRCtrl* fluorescence signal in the orthotopic tumor tissues. We then used RT-PCR to semi-quantitatively detect *let-7a* levels in the tumor and adjacent hepatic tissues, and found that *let-7a* was significantly up-regulated in the tumor tissues but only slightly up-regulated in the

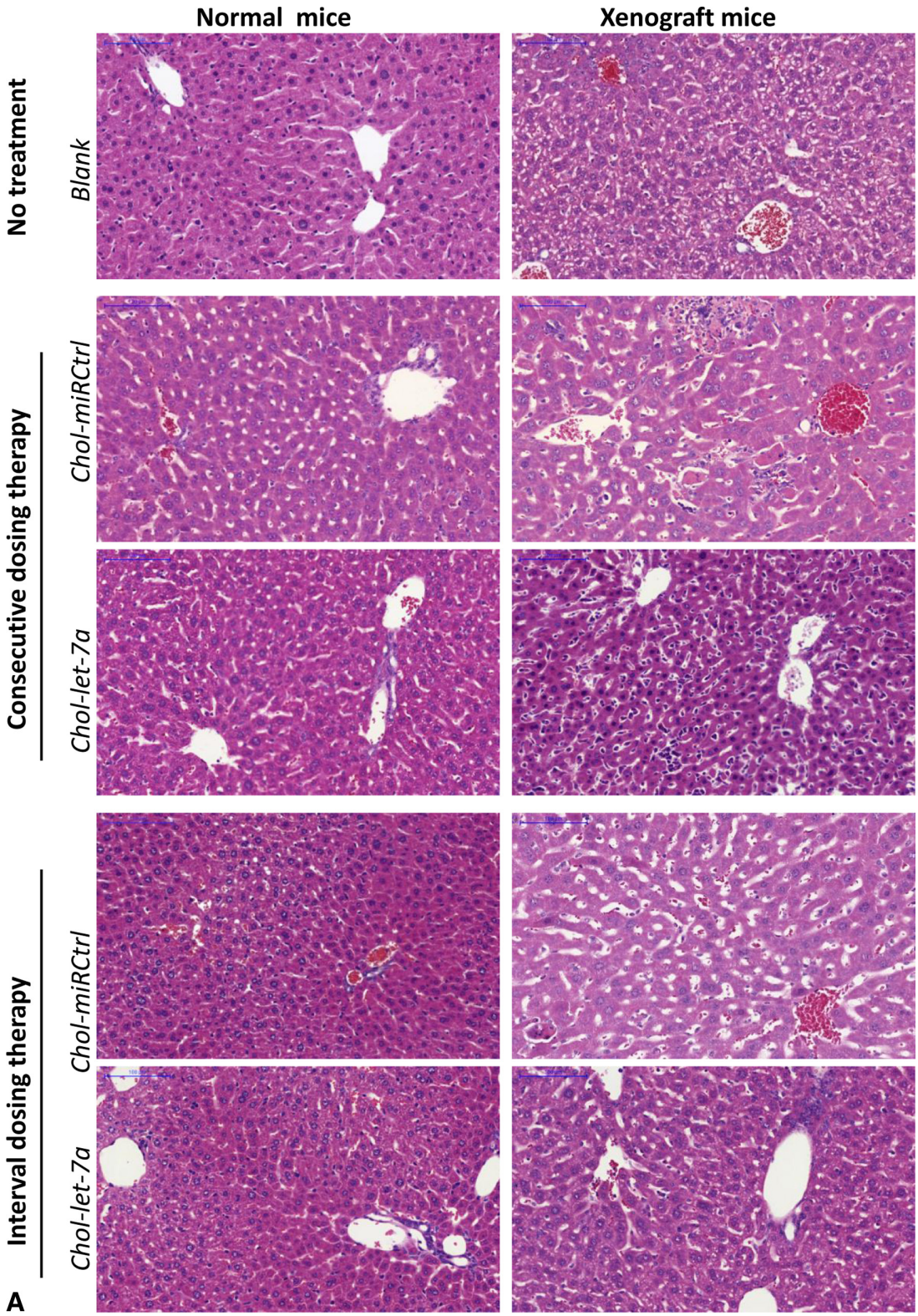

Figure 5. Changes in the liver and kidney after intermittent treatment with *Chol-let-7a* or *Chol-miRCtrl.* Mice with orthotopic xenografts and normal nude mice were injected with intermittent dosing of *Chol-let-7a, Chol-miRCtrl,* or saline (blank), and compared the effects of the molecules on hepatic and renal tissues and cells under light microscope (LM) and transmission electron microscopy (TEM). Here show the findings of histopathological and ultrastructures features in livers and kidneys under LM and TEM to those from mice that received the continuous dosing regimen. The results suggest that features are similar however at milder levels after intermittent dosing treatment than those observed in the mice that received the continuous dosing regimen. (A) Histopathology of the liver after continuous and intermittent therapy (LM). The images show areas of relatively normal liver tissue with no mass necrosis under hematoxylin-eosin staining. Scale bars=100 μm. (B) Glomeruli and tubular interstitia in xenograft and normal mice after intermittent therapy (TEM). Scale bars=2 μm.

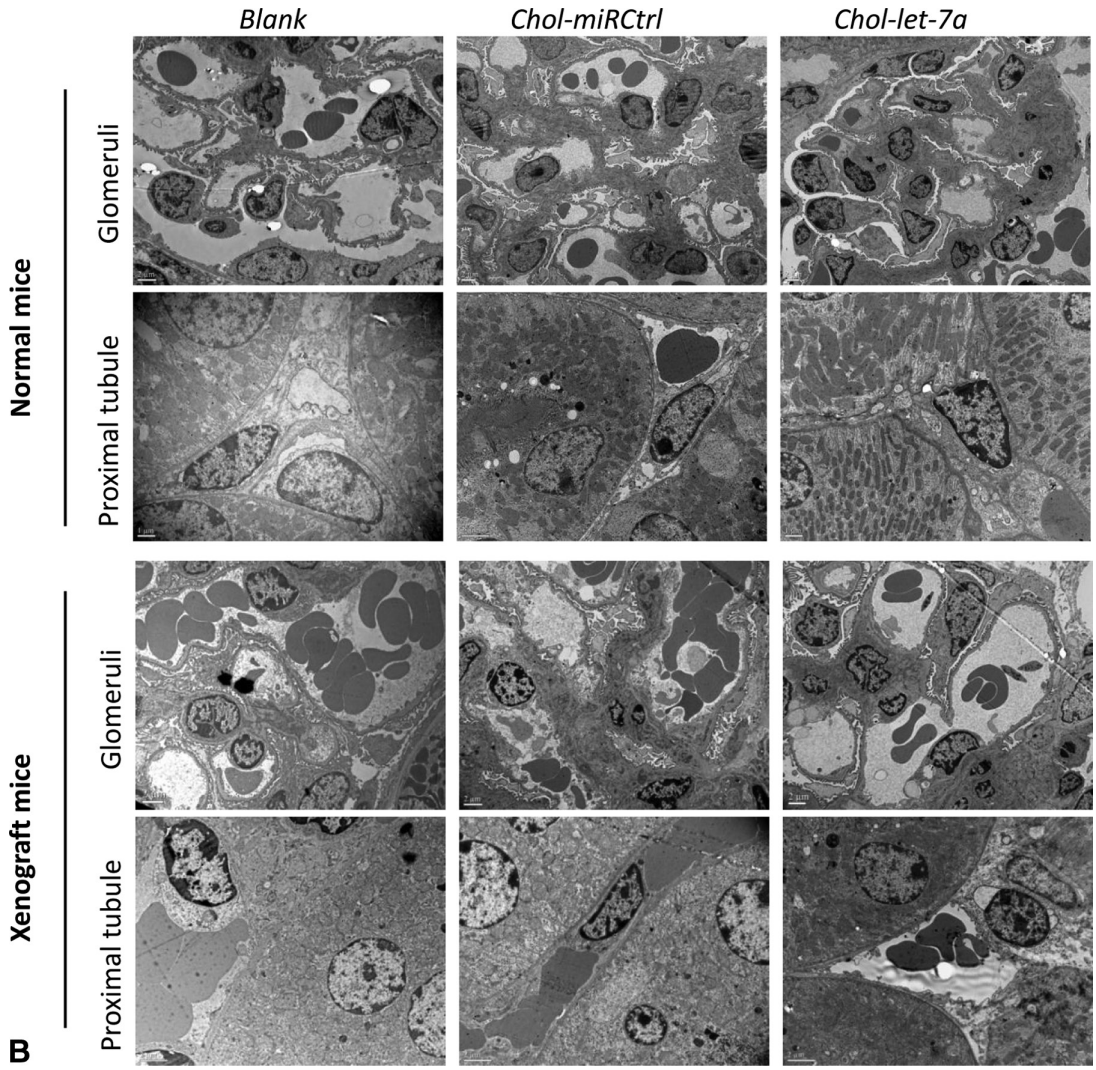

Figure 5. Continued

paracancerous hepatic tissues. These results suggest that there is no major risk of *let-7a* up-regulation in healthy liver tissue having off-target effects.

Potential explanation for the delayed urinary excretion of cholesterol-conjugated molecules seen in the xenograft mice

The specific pattern of kidney toxicity and injury of a drug, xenobiotic, or chemical is dependent on many factors, such as its physiochemical properties (eg, low intrinsic solubility), dose, toxicokinetic properties, renal clearance profile, metabolic attributes, and length of exposure.[20] In this study, we were unable to determine the mechanism of the damage induced by the conjugates. We assessed morphological and ultrastructural tissue changes, as well as conjugate distribution and excretion, to determine why excretion of the cholesterol-conjugated molecules was delayed. There were no obvious differences in the *Chol-let-7a* and *Chol-miRCtrl* fluorescence in the liver and kidney of normal mice. However, in the xenograft mice, especially the *Chol-miRCtrl* and blank xenograft control groups, the fluorescence signals in the kidney decreased slowly and were still partially present at 72 hours post-injection. We believe that the delayed excretion was due primarily to kidney injury and inflammation, which resulted from orthotopic tumor growth.

A previous study reported that kidney parenchyma is especially vulnerable to the pro-inflammatory response to infection, and thus tissue damage, because it receives approximately 25% of the cardiac output.[14] Serum cytokine levels in this study confirmed this to some extent. In normal mice, cytokine levels were not altered by *Chol-let-7a* or *Chol-miRCtrl* treatment. The abundance of four cytokines was significantly increased in the xenograft mice compared with the normal control mice. However, the cytokine levels were significantly reduced after *Chol-let-7a* treatment. In addition, hepatic inflammation and necrosis were also decreased in the *Chol-let-7a*-treated xenograft mice. Thus, the cytokine levels seemed to be consistent with tumor size, degree of inflammation, and necrosis in the three xenograft groups. These results further suggest that the up-regulation of cytokines and inflammation were primarily associated with xenograft growth, rather than *Chol-let-7a*. Thus, the inhibition of kidney-mediated excretion seen in the

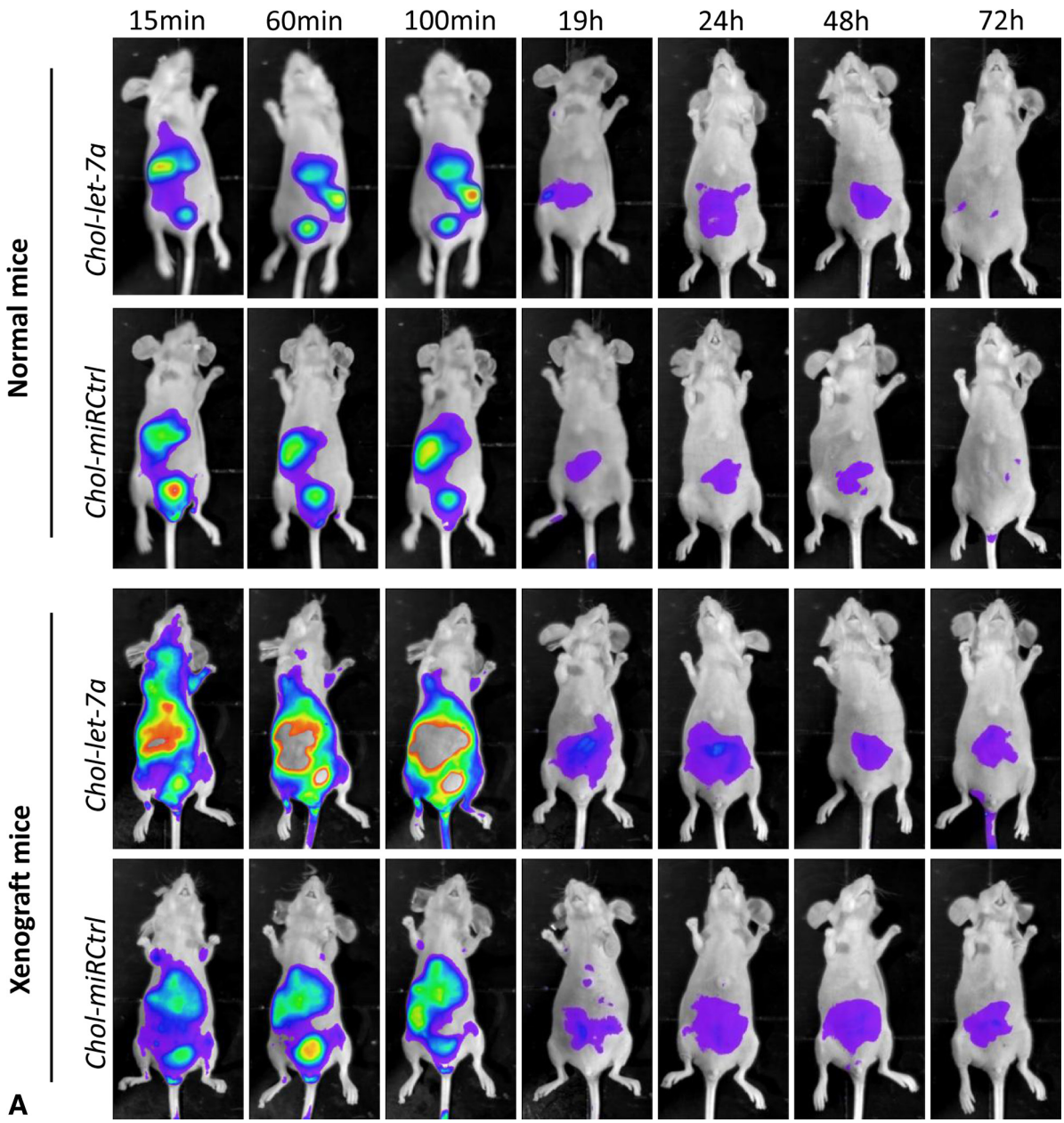

Figure 6. *let-7a* distribution and abundance levels in xenograft tumors and hepatic tissues after *Chol-let-7a* treatment. The distribution of *Chol-let-7a* and *Chol-miRCtrl in vivo* was examined by whole-animal imaging and frozen-sections under confocal and phase fluorescence microscopy observation. *let-7a* abundance in orthotopic tumors, corresponding paracancerous hepatic tissue, and normal liver tissue from healthy nude mice was semi quantitative detected by reverse transcription-polymerase chain reaction (RT-PCR). Whole-animal imaging and frozen-sections observation suggest that the cholesterol-conjugated molecules target to xenograft tumor and liver tissues. RT-PCR confirmed the situation. Whole-animal imaging suggests that kidney function of the xenograft mice was affected; excretion of the cholesterol-conjugated molecules was delayed. (A) Cy5-labeled *Chol-let-7a* and *Chol-miRCtrl* distribution observed from belly (Ventral whole-animal images). (B) Cy5-labeled *Chol-let-7a* and *Chol-miRCtrl* distribution observed from back (Dorsal whole-animal images). The signal strength increases as the color shifts from purple to blue, green, yellow, and red. (C, D) Overall fluorescence levels in the liver (C) and kidney (D) of normal and xenograft animals. The representative average overall signal levels from all groups are shown (n=2 mice per cohort). *Chol-let-7a-N: Chol-let-7a-treated* normal mice; *Chol-miRCtrl-N: Chol-miRCtrl-treated* normal mice; *Chol-let-7a-X: Chol-let-7a-treated* xenograft mice; *Chol-miRCtrl-X: Chol-miRCtrl-treated* xenograft mice. (E) *Chol-let-7a* and *Chol-miRCtrl* distribution in orthotopic tumor tissue and liver tissue. Sections taken 2 hours after injection with *Chol-let-7a* or *Chol-miRCtrl* were observed by confocal and phase fluorescence microscopy. The fluorescent confocal micrographs show *Chol-let-7a* or *Chol-miRCtrl* in the orthotopic tumor tissue and tumor-adjacent liver tissue. Original magnification: 40×. (F) *Chol-let-7a* and *Chol-miRCtrl* distribution in orthotopic tumor and other organ tissue in normal and xenograft mice. Fluorescence was observed 2 hours after injection with *Chol-let-7a* or *Chol-miRCtrl.* 0: tumor; 1: liver; 2: kidney; 3: heart; 4: lung; 5: spleen; 6: pancreas. The signal strength increases as the color shifts from purple to blue, green, yellow, and red. (G) *Let-7a* abundance in xenograft tumor tissue and adjacent liver tissue as determined by real-time PCR. Using miRNA-specific primers, relative *let-7a* levels were calculated using the comparative cycle threshold (CT) method ($2^{-\Delta\Delta CT}$ method), with *let-7a* expression normalized to U6. The results shown represent the mean and standard error from three independent experiments. $^{**}P<0.01$ (Student's *t*-test).

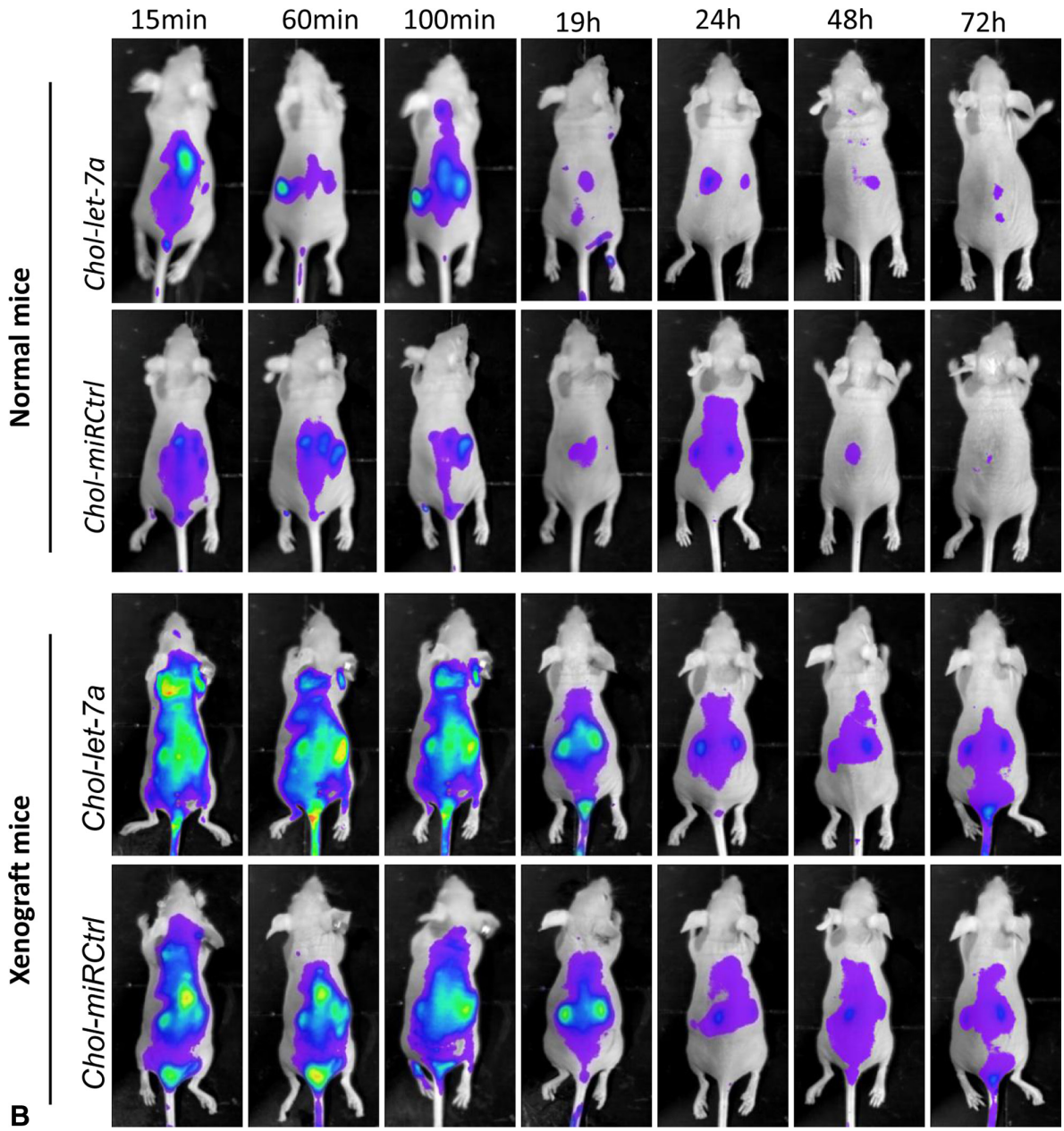

Figure 6. Continued

xenograft mice most resulted from tumor growth, not toxicity of the cholesterol-conjugated molecules. Moreover, the results showed that *Chol-let-7a* treatment could alleviate renal injury by down-regulated cytokines indirectly through inhibiting tumor growth.

Limitations

In this study, the modification with cholesterol-conjugated molecules may function as miRNA, as well as ds-siRNA that could not be divided completely. We only analyzed and discussed based on miRNA functions.

Fluorescence patterns were only analyzed beginning at 100 minutes post-injection and continuing until 19 hours post-injection, owing to experimental limitations. Although this time period allowed us to roughly estimate the *in vivo* distribution and metabolism of these molecules, as well as observe the delay in urinary excretion, it did not enable us to track the complete roadmap of these molecules in the tumor and hepatic tissues.

Owing to the limitations of the experimental conditions, serum cytokines were examined using methods and devices designed for clinical use. In addition, the samples from each group were pooled for testing; thus, the results may not reflect the actual situation.

Conclusions

Both continuous and intermittent dosing with *Chol-let-7a* resulted in successful delivery of the conjugate to xenograft

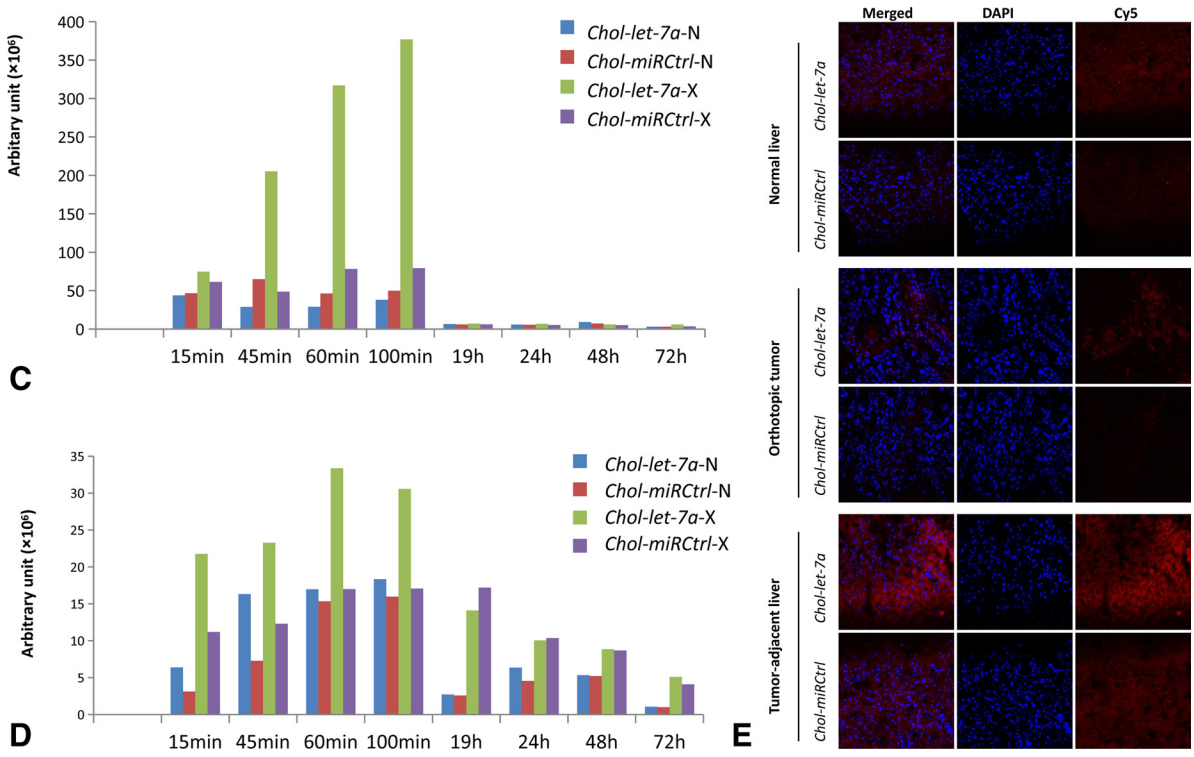

Figure 6. Continued

tumor tissues, as well as up-regulation of *let-7a* levels, and significantly inhibited tumor growth and metastasis.

Chol-let-7a treatment induced some non-specific liver and kidney damage, including diffuse sinusoidal dilatation with or without structural damage and sinusoidal lining cell hyperplasia in livers, and mild membrane hyperplasia in dilated or edematous glomerular capillaries and the tubular interstitium, often accompanied by the presence of inclusion bodies in the glomerular endothelial cells.

Chol-let-7a did not seem to have any severe off-target effects. In addition, it alleviates the inflammation and congestion caused by the tumor itself by inhibiting tumor growth.

Using an intermittent dosing regimen to reduce the damage associated with *Chol-let-7a* while maintaining satisfactory antitumor efficacy could be a useful strategy in future studies, and potentially clinical use.

Acknowledgments

The authors thank Mrs. Huimin Zhao, Wenyu Hao, and Huanxian Cui from the Centre for Experimental Animal Research (CEAR), Institute of Basic Medical Sciences, CAMS/PUMC, as well as Xiao Yang (VisualSonics, Inc. Beijing, China) and Yi Gao (Berthold, Beijing, China) for the technical support. We also thank Dr. Wei-Min Tong for his constructive suggestions in support of this study. The authors thank Dr. Xingyi Hang and Ms. Jiahui Liu for their assistance with statistical analysis.

Author contributions

JG initiated the project. JG and ML analyzed data, wrote the manuscript, and performed most of the experiments. YX performed ultrasonic analysis. XL, WD, and YH performed electronic microscopic analysis. LZ, XD, TY, SG, XL, and YL performed molecular imaging, western blot, immunohistochemi-cal staining, hematoxylin-eosin staining, and analysis. All authors read and approved the final manuscript.

Financial support

This work was supported partly by the National Human and Health Scientific Data Sharing Platform, Clinical Center of China (No. 2004DKA20240-2014), and National Program funded by the Ministry of Science and Technology of China (No. 2015KJRK1L01). The content is solely the responsibility of the authors and does not represent the official views of the funding agencies.

Institutional review board statement

The experiments were approved by the Institutional Research Board of Peking Union Medical College Hospital.

Conflicts of interest

The authors declare that they have no conflicts of interest.

Editor note: JG is an Editorial Board member of *Journal of Bio-X Research*. She was blinded from reviewing or making decisions on the manuscript. The article was subject to the journal's standard procedures, with peer review handled independently of this Editorial Board member and their research groups.

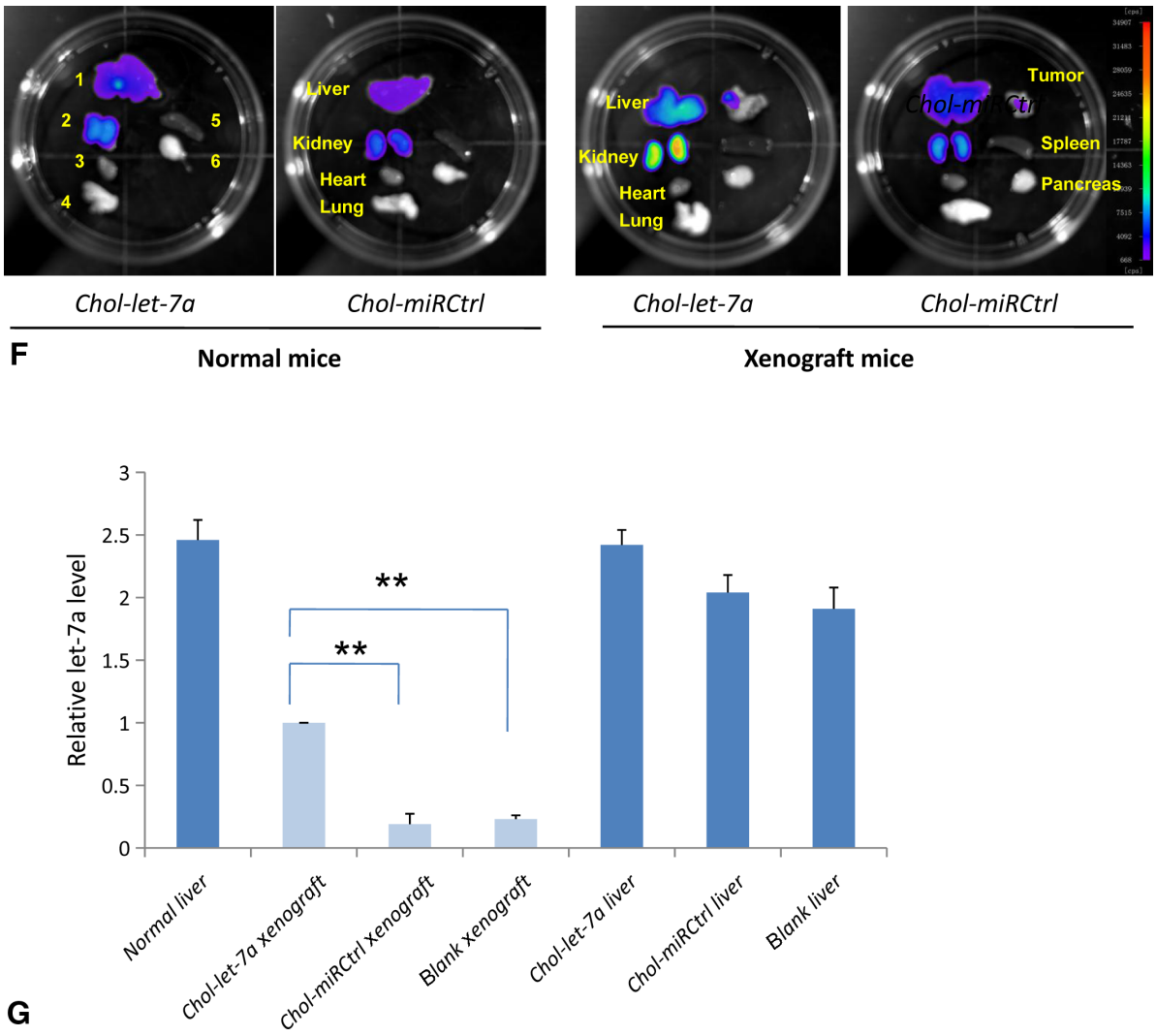

Figure 6. Continued

References

[1] Bray, F, Ferlay, J, Soerjomataram, I, et al. Global cancer statistics 2018: GLOBOCAN estimates of incidence and mortality worldwide for 36 cancers in 185 countries. CA Cancer J Clin 2018;68:394–424.

[2] Chen, W, Zheng, R, Baade, PD, et al. Cancer statistics in China, 2015. CA Cancer J Clin 2016;66:115–132.

[3] Zhu AX, Finn RS, Edeline J, et al. Pembrolizumab in patients with advanced hepatocellular carcinoma previously treated with sorafenib (KEYNOTE-224): a non-randomised, open-label phase 2 trial. Lancet Oncol 2018;19:940–952.

[4] Otsuka M, Kishikawa T, Yoshikawa T, et al. The role of microRNAs in hepatocarcinogenesis: current knowledge and future prospects. J Gastroenterol 2014;49:173–184.

[5] Iqbal MA, Arora S, Prakasam G, et al. MicroRNA in lung cancer: role, mechanisms, pathways and therapeutic relevance. Mol Aspects Med 2019;70:3–20.

[6] David, S, Meltzer SJ. MicroRNA involvement in esophageal carcinogenesis. Curr Opin Pharmacol 2011;11:612–616.

[7] Takahashi, RU, Prieto-Vila, M, Kohama, I, et al. Development of miRNA- based therapeutic approaches for cancer patients. Cancer Sci 2019; 110:1140–1147.

[8] Wei L, Wang X, Lv L, et al. The emerging role of microRNAs and long noncoding RNAs in drug resistance of hepatocellular carcinoma. Mol Cancer 2019;18:147.

[9] Kaczmarek JC, Kowalski PS, Anderson DG. Advances in the delivery of RNA therapeutics: from concept to clinical reality. Genome Med 2017;9:60.

[10] Bajan S, Hutvagner G. RNA-Based therapeutics: from antisense oligonucleotides to miRNAs. Cells 2020;9:137.

[11] Rupaimoole R, Slack FJ. MicroRNA therapeutics: towards a new era for the management of cancer and other diseases. Nat Rev Drug Discov 2017;16:203–222.

[12] Giordano S, Columbano A. MicroRNAs: new tools for diagnosis, prognosis, and therapy in hepatocellular carcinoma? Hepatology 2013;57:840–847.

[13] Morishita A, Masaki T. miRNA in hepatocellular carcinoma. Hepatol Res 2015;45:128–141.

[14] Liu YM, Li X, Xia Y, et al. Cholesterol-conjugated let-7a miRNA mimics: promising tools for HCC systemic therapy. RNA Disease 2015;2:630.

[15] Liu YM, Xia Y, Dai W, et al. Cholesterol-conjugated let-7a mimics: antitumor efficacy on hepatocellular carcinoma in vitro and in a preclinical orthotopic xenograft model of systemic therapy. BMC Cancer 2014;14:889.

[16] Feldmann G, Fendrich V, McGovern K, et al. An orally bioavailable small-molecule inhibitor of Hedgehog signaling inhibits tumor initiation and metastasis in pancreatic cancer. Mol Cancer Ther 2008;7:2725–2735.

[17] Livak KJ, Schmittgen TD. Analysis of relativegeneexpressiondata using real-time quantitative PCR and the 2(-DeltaDeltaC(T)) Method. Methods 2001;25:402–408.

[18] Radi ZA. Kidney pathophysiology, toxicology, and drug-induced injury in drug development. Int J Toxicol 2019;38:215–227.

[19] Kumar S. Oral contraceptive-induced hepatic sinusoidal dilatation. Dig Liver Dis 2015;47:e10.

[20] Geller SA, Petrovic LM Geller SA, et al. Effects of drugs and toxins on the liver. Biopsy interpretation of the liver. 2nd ed. Baltimore: Wolters Kluwer Health Lippincott Willians & Wikin; 2009;136–149.